Philippine Journal of Science
152 (1): 291-306, February 2023
ISSN 0031 - 7683
Date Received: 31 May 2022

Development of Pag-asa Reefs, West Philippine Sea: Role of Relative Sea Level Change and Wave Exposure

Denise Faye S. Janer[1,2]*, Mary Rose P. Gabuyo[1,2], Anne Drew V. Carrillo[1,2], Paolo Emanuel Y. Co[1,2], Aiko Love B. del Rosario[1,2], Michael Jayson S. Morata[1,3], Jelee B. Dayao[3], Maylord M. de Chavez[3], Dennis Arsenio B. Bringas[3], Cesar L. Villanoy[1,2], and Fernando P. Siringan[1,2]

[1]Pag-asa Island Research Station, Kalayaan Group of Islands, Kalayaan, Palawan 5322 Philippines
[2]The Marine Science Institute, University of the Philippines Diliman, Velasquez Street, Quezon City 1101 Philippines
[3]National Mapping and Resources Information Authority, Fort Andres Bonifacio, Taguig City 1634 Philippines

Atoll reefs are associated with subsiding regions. In the West Philippine Sea, the Kalayaan Island Group is an emergent feature of the region's atoll reefs. In this study, we established the long-term rate of subsidence in the Pag-asa Atoll Reefs by indicators of sea level positions on the seafloor and in Pag-asa Island. For submerged indicators of paleo-sea levels, a multibeam bathymetry with a 5-m resolution was used as the primary data source. Four pairs of submerged terraces and scarps, interpreted as former coral reef flats and reef fronts, respectively, were mapped. The terraces, PARa-d, from shallowest to deepest, occur at depth ranges of 7–10, 36–45, 82–90, and 115–120 m. The step-like morphology of the slopes off Pag-asa is likely due to the backstepping of reefs during the overall rise of sea level from the Last Glacial Maximum (LGM). Terraces PARa-d are interpreted as records of reef re-establishments during the stillstand periods following meltwater pulse event (MWP)-1C, MWP-1B, MWP-1A, and MWP-2B/2A. There is no clear morphological indicator of coral terraces that can be attributed to the LGM period. Variation in the widths and depths of the terraces between the leeward and windward sides of the island is also observed. Greater wave exposure appears favorable for coral reef terrace growth in Pag-asa, except for deeper terraces. The possible absence of the deepest terrace on the north side and an LGM terrace is attributed to possible thinner coral reef accretion due to the combination of cooler waters and possible swifter winds prior to 14 kyr. Correlation of the terrace depths and beach rock elevations as Pag-asa with the paleo-sea level of correlative stillstand events indicate long-term subsidence of 1.2 mm/yr between 15–12 kyr that declined to 0.3 mm/yr between 12 kyr to present. With sea level rise due to global warming and continuing subsidence, Pag-asa Island is threatened by coastal erosion, more frequent inundation, and groundwater salinization that needs to be addressed through proper adaptation practices.

Keywords: backstepping, sea level, submerged terraces, subsidence, wave exposure, West Philippine Sea

*Corresponding author: dsjaner@msi.upd.edu.ph

INTRODUCTION

Atolls are annular mid-ocean coral reefs surrounding a central lagoon (Cabioch *et al.* 2010). They occur extensively across the Indo-Pacific region characterized by permanently warm surface waters due to the Indo-Pacific Warm Pool (de Deckker 2016). In tropical areas, modern or fossilized coral reefs form coral reef terraces (Pedoja *et al.* 2018). The International Hydrographic Organization defines "terrace" as "a flat or gently sloping surface that is bounded along one edge by a steeper descending slope and along the other by a steeper ascending slope." Coral reef terraces are formed close to sea level and thus they serve as a good proxy for the paleo-sea level at the time of their formation. Reef morphology is dependent on both intrinsic and extrinsic factors, although the latter has been regarded as the more dominant driver of varying morphologies and complex reef stratigraphy (Pastier *et al.* 2019). Extrinsic factors include – but are not limited to – eustatic sea level changes, tectonic motions, antecedent topography, dissolution, and oceanographic factors (Camoin and Webster 2015). The basic modes of reef response introduced by Neumann and Macintyre (1985) (*i.e,* keep-up, catch-up, and give-up by drowning) suggest possible outcomes in reef morphology with varying rates of sea level rise. Another pattern of reef development is progradation or the lateral growth of reefs, which occurs during periods with relatively stable sea levels (Cabioch *et al.* 2010). Later, the backstepping response was recognized from Pleistocene and Holocene reefs in the Caribbean (Blanchon and Shaw 1995) as a means for reefs to respond to rapid sea level changes, which produce a stair-like morphology of terraces. The backstep mechanism occurs when there is sustained sea level rise and when the substrate is suitable that can lead to the landward reestablishment of new reefs and drowning of reefs at the deeper site (Blanchon 2011). This mechanism is also observed in subsiding regions as magnified relative sea level rise triggers reef backstepping (*e.g.* Hawaii, Faichney *et al.* 2009).

The mechanisms mentioned above are reflected in the long-term vertical coral growth in atoll reefs as a response to the subsidence of its basement. In the Pacific, deep drilling results at the reef rim of Enewetak Atoll in the Marshall Islands show that the carbonate accumulations are more than 1400 m (Ladd *et al.* 1953). As the atoll subsides, the carbonate accumulates as a product of periods where reefs grew by either catch-up or keep-up mechanisms due to relative sea level rise. Thus, atoll reefs are good sites to observe coral reef growth response to changing relative sea levels and to reconstruct them.

Aside from tectonic-driven relative sea level changes, wave energy also significantly influences reef growth. In the reefs of the Hawaiian Islands, the vertical coral accretion rate is more significant in wave-sheltered sites (*e.g,* Grigg 1998). However, in certain scenarios, higher-energy reefs demonstrate greater lateral accretion and framework resistance than medium-energy reefs (Hongo and Kayanne 2009). The effect of wave exposure is further associated with spurs and grooves that are commonly found on forereef areas. Energetic incident waves modify the growth of reefs so that linear spurs form when coral colonies coalesce due to continued unidirectional growth towards the direction of incident waves (Shinn 1963).

High-resolution bathymetry data has been used by previous studies to determine paleo-sea level trends (*e.g,* Great Barrier Reef, Abbey *et al.* 2011). In interpreting reef morphology, it is important to note that drivers of relative sea level change are significant at different scales (Horton *et al.* 2018). For instance, the consequence of tectonic-related events, such as subsidence, can be observed uniformly even at distances in the order of 10^3 m. Contrastingly, this cannot be true for other factors such as wave energy. At scales less than 10^3 m, variations in reef morphology due to wave energy may manifest. Hence, the spatial resolution of the data must be considered in reef morphology studies.

In this paper, we use mainly a 5-m-resolution multibeam bathymetry data to characterize the seafloor morphology of Pag-asa Reefs. We aim to establish the development of the atoll systems on the northwest fringe of the continental shelf of offshore mainland Palawan since about 18,000 years ago. We explore the role played by wave exposure and antecedent topography, as well as the duration of stillstands and periods of relative sea-level stability in reef development. Furthermore, we provide an estimate of the long-term atoll subsidence rate using the morphology of submerged reefs and how it interacted with the effects of meltwater pulse events (MWPs) in modifying the relative sea level history of the area.

Study Area

The Pag-asa Reefs (or Pag-asa), which refer to both West Pag-asa Atoll Reef (wPAR) and East Pag-asa Atoll Reef (ePAR), are atoll reefs located at the northwest part of the Kalayaan Group of Islands (KIG) in the West Philippine Sea, about 500 km away from mainland Palawan (Figure 1A). The territorial West Philippine Sea refers to the Philippine maritime areas within the geologic South China Sea basin that are within the country's Exclusive Economic Zone and extended continental shelf according to the United Nations Convention on the Law of the Sea. Specifically, this study looked at the seafloor morphology surrounding wPAR and ePAR (Figure 1B). Within wPAR is Pag-asa Island, where the Pag-asa Island Research Station is located. Tide gauge data between April–June 2017 yielded a tidal range of 0.86 m.

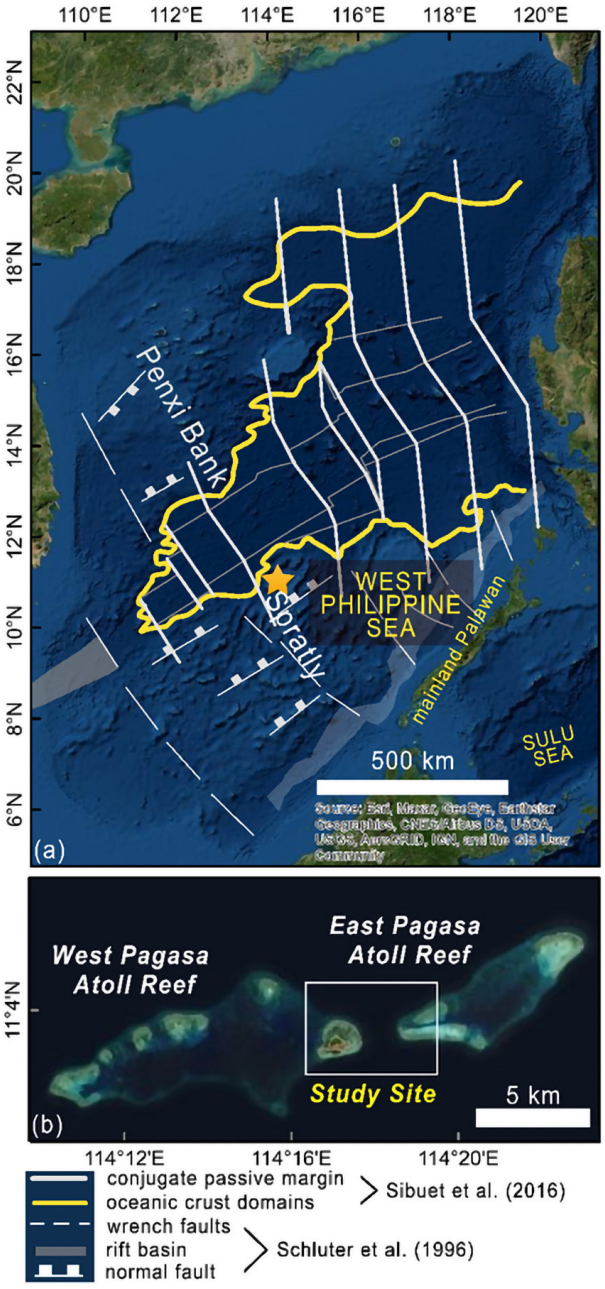

Figure 1. [A] Structural map of the South China Sea Basin adapted from Schluter *et al.* (1996) and Sibuet *et al.* (2016). Thick yellow line shows the continental-oceanic boundary. Pag-asa Reefs (star) overlies the fringe of thinned continental margin. [B] The Pag-asa Reefs (or Pag-asa), West Pag-asa Atoll Reef (wPAR) and East Pag-asa Atoll Reef (ePAR). The background satellite imagery in the maps is taken from Google Earth. The extent of the study site is enclosed in the box.

Regional Setting

The South China Sea (SCS) basin is a marginal basin located west of the Philippine Mobile Belt. The central part of the SCS basin is underlain by oceanic crust, enveloped by thinned continental crusts to the north and south (Sibuet *et al.* 2016). The rifting of the oceanic basin initiated around 33 Ma ago along the Ulugan Bay Fault north of mainland Palawan, then progressively shifted towards the west. This formed a discontinuous ridge axis transected by seafloor spreading lineaments and fault zones that are conjugate segments of passive margins (Sibuet *et al.* 2016). The Spratley Islands–Penxi Bank segment, which crosses Pag-asa, is a former plate boundary during the third phase of the opening of SCS at 27–22 Ma (Sibuet *et al.* 2016) (Figure 1A). Hence, the crust underlying Pag-asa is located along the fringes of the thinned continental margin. This part of the offshore Palawan shelf is a pure-sheared terrane characterized by extensional faults that are initiated during episodes of stretching and thinning of the underlying continental crust (Schlüter *et al.* 1996). The linear bathymetric highs that make up the Spratly Islands (partly KIG), are half-graben structures trending northeast-southwest parallel to the orientation of normal faults in the area (Schlüter *et al.* 1996). It can be inferred that since their formation, this same extensional regime has influenced the development of the atoll systems within KIG, including the Pag-asa Reefs.

MATERIALS AND METHODS

Multi-beam Bathymetry

The primary data used in this study is multi-beam bathymetry provided by the National Mapping and Resource Information Authority (NAMRIA). The extent of the data is within the quadrangle that stretches from $11^0$5.676' N, $114^0$16.020 'E to $11^0$0.336' N, $114^0$21.786' E. This covers only the eastern portion of wPAR and the western portion of ePAR. The density of the multibeam data points was statistically estimated to be 40 m and was reprocessed to produce a bathymetry map with a spatial resolution of 5 m.

Single-beam and Side-scan Surveys

Single beam and side-scan surveys were also conducted around Pag-asa Island, which is at the east end of the wPAR, to cover the shallower areas. In 2017, NAMRIA acquired single-beam bathymetry data on the shallow reef flat areas around Pag-asa Island and within the west end of ePAR along survey tracks spaced at 50 m. Single-beam bathymetry and sidescan data were also acquired around Pag-asa Island in April 2021 and February 2022. The Humminbird 698ci HD SI Combo, operating at 455 kHz with dual sonar frequency of 200/83 kHz, was able to record depths of up to 300 m while side-scan images were recorded within a total bottom coverage of 80 m at a maximum depth of 50 m. The transducer was mounted at the side of a rubber boat with a metal pole and submerged ~

0.3 m below the water surface. A total of 25 perpendicular profiles distributed between the immediate offshore areas to the north and south of Pag-asa Island were acquired with three tie lines. The perpendicular tracks were spaced 300 m, whereas the tie line tracks were about 100 m apart. The datasets from 2017, 2021, and 2022 were combined to interpolate a 10-m resolution bathymetry of the shallow areas within the study site. Since the data points are derived by a single beam, the data coverage is limited by the spacing of the survey track. Hence, the resolution of the shallow bathymetry is not sufficient to observe for continuity of seafloor features and was mainly used to generate individual profiles along the tracks.

Mapping of Paleo-sea Level Indicators on the Island

We traversed the island along several transects and circumscribed the shoreline to locate possible paleo-sea level indicators on the island such as wave-cut terraces, marine notches, emergent beach rocks, and framework reefs. We used a hand-held GPS that is accurate to within 3 m to mark the locations of features found. Their elevations were measured by ground leveling survey and reported with respect to mean sea level (msl). Fixed NAMRIA benchmarks on the island were used as references during ground leveling.

Surface Wind Satellite Observations

Wind data was used as a proxy to infer wave exposure variations in Pag-asa. This study used the available EU Copernicus Marine Service Information time series of monthly-averaged surface wind data as a proxy for wave exposure (https://doi.org/10.48670/moi-00181). The coverage of the wind satellite observations is from 05 May 2007–31 Dec 2020. The predefined variables, wind speed, and wind stress were used to generate wind rose diagrams in MATLAB. The calculation is based on a single point within Pag-asa with coordinates 11.12500 N, 114.37500 E using Wind Rose codes (Pereira 2022).

RESULTS

Terrace Morphology

The bathymetry data shows the fore reef slopes surrounding Pag-asa Island in wPAR and ePAR as well as the channel that separates the two reefs (Figure 2A). For the following discussion, *wPAR*- and *ePAR*- will be used as prefixes to indicate the location of the terrace being discussed (*i.e, wPARa* and *ePARa* refer to the trace of terrace *PARa* in west Pag-asa Atoll Reef and east Pag-asa Atoll Reef, respectively).

A total of 183 transects across the reef flat to the 200-m contour reveal the presence of at least four submerged terraces (*terraces PARa-d*). The stacked profiles of the terraces show distinct variations in terms of depth, width, extent, and slope (Figure 2B). The three shallower terraces, terrace *PARa-c*, are the most well-defined and continuous across the forereef. In contrast, terrace *PARd,* the deepest terrace, is only distinct towards the southern slopes. This is true for both wPAR and ePAR. The overall range of terrace depth is in the order of more than 10 meters, defined by relatively rugged bathymetry, probably due to shallow catch-up and keep-up coral growth and erosion. To eliminate the variation caused by these shallow features, the depth range where the terrace surfaces converge (as seen on the stacked profiles, Figure 2B) was assigned for the terraces. For sloping terraces, the depth range for the upper surface was used since it best approximates the paleo-sea level position during the formation of the terraces. Based on this notion, terraces *PARa-d* occur at depth ranges of 7–10 m, 36–45 m, 82–90 m, and 115–120 m respectively. Since terrace *PARd* is not well-defined, its depth range limits correspond to a consistent slope break on the seafloor south of ePAR and wPAR, respectively.

In order to scrutinize the continuity and lateral variation in the morphology of the terraces, surface slope analysis and hillshade visualization of the bathymetry of Pag-asa was done (Figure 3A). On the other hand, to observe small-scale vertical variation within the surface of the terraces, the shallow edge of each terrace was traced to generate a depth profile by using the slope map as a reference (Figure 3B). In terms of width and extent, terrace *PARa* is the widest terrace. For example, terrace *wPARa* is more than 1 km at most on the north side and decreases to a width of only 300 m on the south. The slope of terrace *PARa* is almost flat for both the north and south side**,** bounded by scarps with a slope of 55–60° at the seaward edge. Meter-scale mounds provide irregularity in the terrace profile. The depth range of terrace *PARa* in both atolls is considerably uniform, except for the southern *ePARa* terraces which occur consistently at depths shallower than 10 m, whereas terrace *PARb and PARc* show common patterns in morphology. At the transition from the northern to the southern side of the reefs, the terraces follow deeper contours when facing the channel separating the two atoll reefs (Figure 3B). Both of the terraces reach maximum width at the slopes facing this channel, especially *ePARb* and *ePARc* at 200 and 230 m wide, respectively. The deeper bounding scarps of terrace *PARb and PARc* are gentler along the channel, at only 57° and 28° *versus* the steeper slopes of 64° and 38° on the north, and 75–80° on the south, respectively. The terrace surfaces of *wPARb-c* themselves are also sloping downward on the south (18° and 36° respectively) and east side (14° and 19° respectively) *versus* their almost flat surfaces on the north

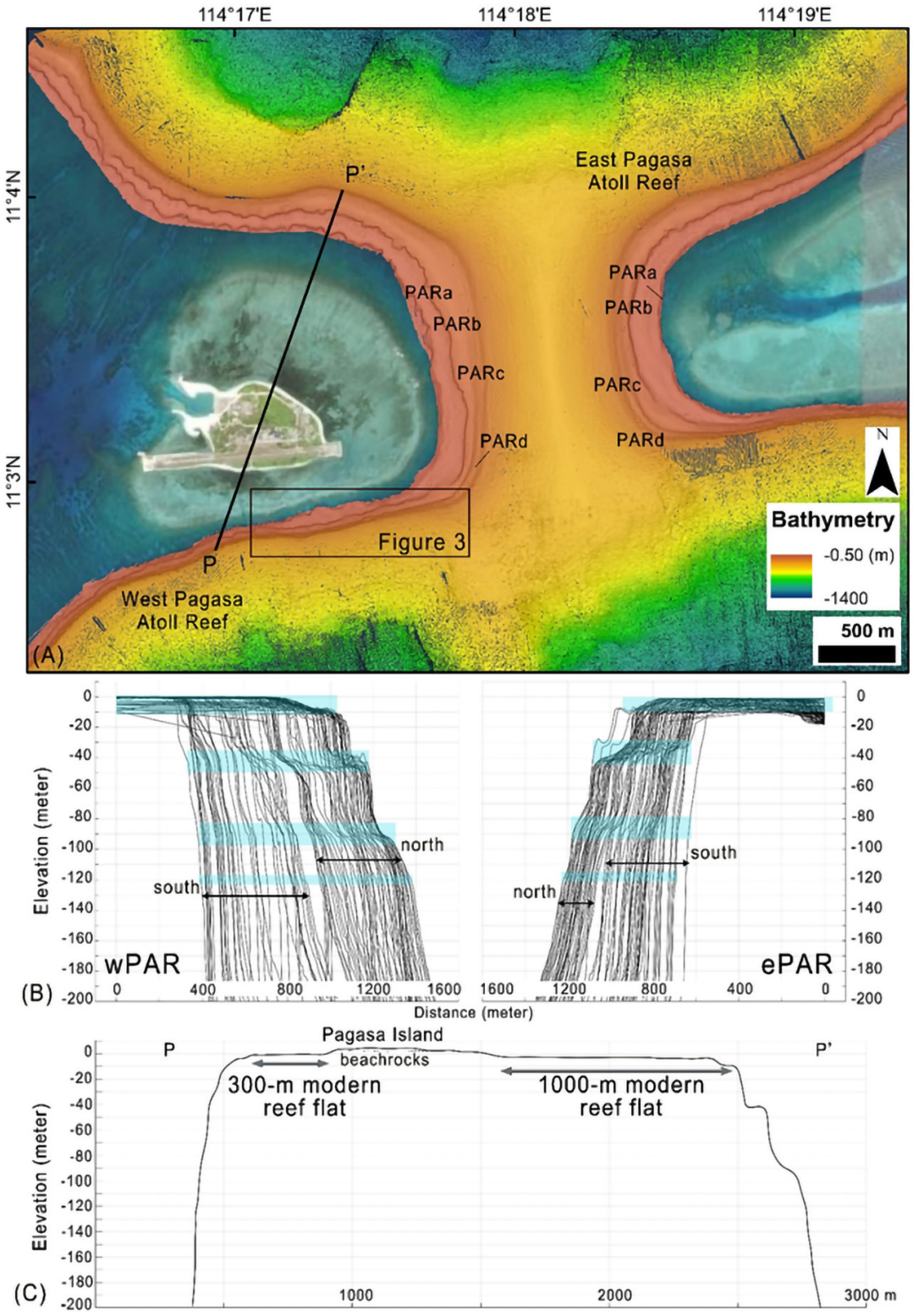

Figure 2. [A] The 5-m resolution bathymetry map of a portion of the Pag-asa Reefs superimposed on a slope map. The 10-m resolution bathymetry of the shallow areas is not shown. [B] Stacked bathymetric profiles on wPAR and ePAR reveal the occurrence of submerged terraces, whose extent is enclosed in blue boxes. [C] A south-north profile of wPAR shows the great difference in the width of extant reef flats between the north and south side of Pag-asa Island. The northern submerged terraces are also more well-defined than the south, whereas terrace *PARd* is only distinct in the south.

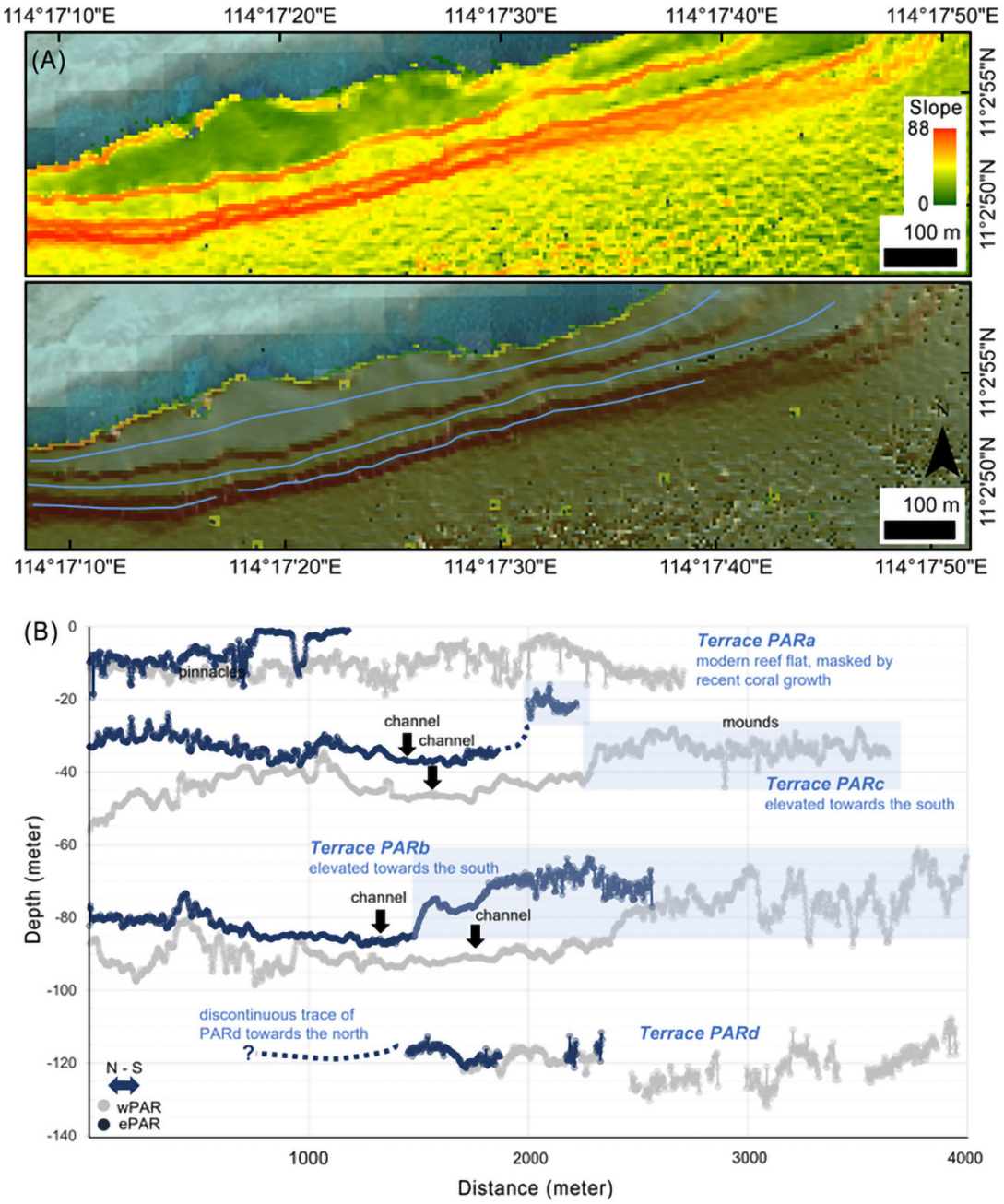

Figure 3. [A] Slope and hillshade visualization of the submerged terraces. The steep slope (red) of the scarps sharply bounds the gentler terrace surfaces (green). The blue lines on the terraces overlain on the hillshade map show how the terrace surfaces were sampled to investigate for depth variation. [B] Depth variation of terraces *PARa-d* traced in both wPAR and ePAR over a distance of 8 and 5 km, respectively. See location in Figure 2A.

(2° and 7° respectively). In contrast, e*PARb*-c terraces are generally flat except for their southern counterparts that slope downwards at 30°. For both *PARb* and *PARc* terraces, their surfaces steeply form at shallower depths towards the south. For *PARb* profiles, several mounds are present on both the north and south sides. In comparison, southern terrace wPARc has mounds with a wide depth range. Although, it is possible that this is a remnant of sampling data points, as the terrace surface becomes too narrow on the south. In ePARc, the mounds are more densely clustered. These features generally lie within a shallower depth range compared to their northern counterparts, which have more uniform but deeper depths.

Lastly, terrace *PARd* is a discontinuous terrace that is present only on the southern side of both atoll reefs (Figure 3B). It is characterized by very narrow sloping surfaces with a maximum width of 40 m. Its surface is sloping down at 25° near the channel and 40° on the south. Near the channel, its seaward scarp is distinctly gentler at 33° and almost instantly steepens to 87° on the south.

Side-scan Observations

Features of the submerged terrace *PARa* surrounding Pag-asa Island in wPAR were imaged in 455 kHz resolution side-scan images (Figure 4). The surface of terrace *PARa* on the north is distinct by the presence of spurs and grooves. In the side-scan, they are rough, linear features with a clear boundary interspersed with smooth channels of low backscatter intensity. The spurs have an average width of 20 m and varied lengths. In satellite images, spurs are 200–300 m long (Figure 4B). They form extensively within the reef front of terrace *PARa* around 900 m away from the shoreline, at depths of 7–10 m. At depths less than 5 m, some spurs are more closely spaced, *i.e.* the channels are very narrow (Figure 4A). The spurs and

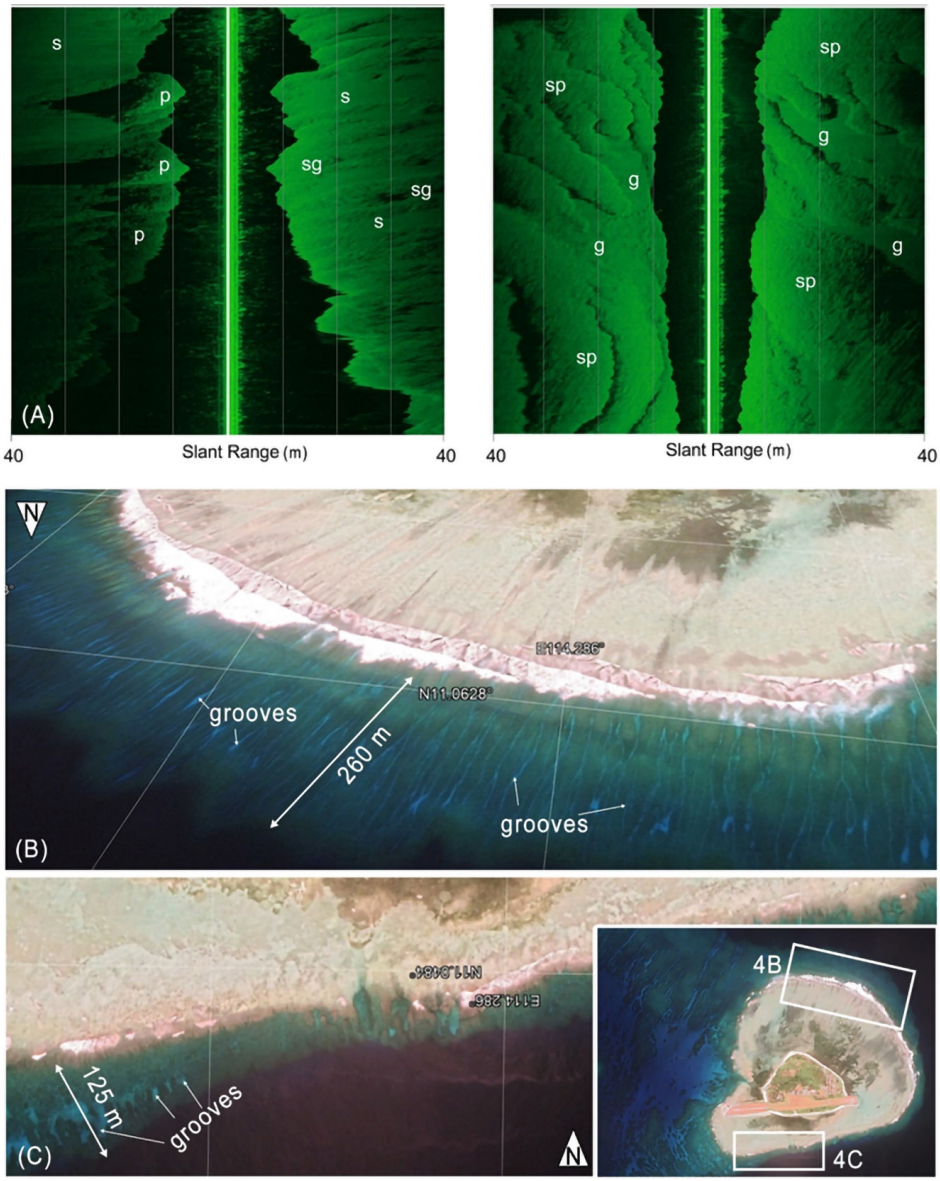

Figure 4. [A] Side-scan images of terrace *PARa* on the north (right) and south (left) reef front of Pag-asa Island. Features are labeled as follows: [s] sand, [sg] seagrass, [sp] spurs, [g] groove, and [p] pinnacle. Satellite image from November 2018 on Google Earth shows spur and grooves on the [B] north and [C] south reef front of west PAR. Some grooves are traced with white outlines on both reef fronts.

grooves terminate at the seaward edge of the terrace, just before the steep slope break. On the south, spurs and grooves are also present on the reef front of terrace *wPARa* but less extensive as seen in satellite images (Figure 4C). In side-scan images, the southern narrow reef flat is composed of sand, patch reefs, pinnacles, and seagrass beds (Figure 4A). The reef pinnacles form steep mounds that rise about 3–10 m above the surrounding seafloor. They are isolated structures and cast a shadow on their trailing edge. Pinnacles are observed on the reef crest of terrace *PARa* on the south, adjacent to the steep slope break at the reef front. Aside from pinnacles, patch reefs are also present in the south. They are clusters of rough low-relief structures with diffuse boundaries. Whereas, seagrass beds are smooth low-relief structures that are interspersed with sand.

Based on a previous survey around Pag-asa Island, dead corals occupy 65% of the benthos (Quimpo *et al.* 2019). In areas with hard coral cover, coral abundance is higher in shallow water reefs (depth range of 8–22 m; within *terrace PARa*), composed of encrusting, massive, and foliose coral morphologies. On the other hand, mesophotic coral ecosystems (depth range of 30–40 m; within *terrace PARb*) have lower coral abundance and are dominantly composed of encrusting corals.

Emergent Beachrocks

Marine notches and emergent coral reef framework materials were not encountered around and across the island. However, beach rock was found outcropping broadly within Pag-asa Island (Figure 5A). This is consistent with the observation of Ong and co-authors (2000). The most continuous beach rock exposure is about 80 m wide and 50 cm thick, at the western portion of the island (Figure 5B). Ground leveling survey indicates that this has a maximum elevation of 2.6 m above the present msl, the highest elevation on the island. The majority of the beach rock exposures are irregularly eroded patches less than 30 cm thick. One exposure, in particular, was carved to function as a garden patch (Figure 5C). The beach rock is composed of loosely cemented medium-coarse carbonate sand particles with pebble-sized coralline clasts. In an excavation area at the central part of the island, the beach rock is approximately 1.5 m thick (Figure 5D). Underneath the beach rock are loose sands. In another part of the island, only about 20 cm thick semi-lithified rusty beach rock layer was observed near the surface in a hole dug for placement of a plastic septic tank during the field visit (not shown in the figure). The hole was dug to about 1.8 m from the surface, hitting mostly sand with a layer of coral and shell fragments close to the bottom.

DISCUSSION

Pag-asa Reef Morphology Response to Deglacial Sea Level Changes

The numerous atolls in the West Philippine Sea indicate widespread subsidence in the region. Subsidence, or tectonic vertical motions in general, is one of the major controlling factors of reef architecture (Pastier *et al.* 2019) and is associated with thick atoll reef sequences (*e.g.* Liu *et al.* 2022). Also, the eustatic sea-level history of the study area is significant to this discussion. We use primarily that of Liu and co-authors (2004) (Figure 6), which is based on a database of radiometrically-dated sea level indicators. Their reconstruction of sea level change identifies six rapid sea level rise events following LGM, which is placed 120 m below the present msl around 19–22 kyr (Liu *et al.* 2004). The rapid rises are attributed to the melting of glaciers, causing MWPs. Immediately following the LGM, two separate short minor pulses of equal magnitude, MWP-2A and 2B are identified by Liu and co-authors (2004). After these events are MWP-1A and -1B with estimated rates of 80 and ~ 25 mm/yr, respectively (Liu *et al.* 2004). This estimate for MWP-1A is much higher than the rate estimated for Barbados reefs (24 mm/yr; Fairbanks 1990). This discrepancy might be due to the contribution of subsidence due to natural compaction typical in delta deposits and or hydro-isostatic response. MWP-1C started around 9.8 kyr BP with a rate of 45 mm/yr over a period of 800 yr (Liu *et al.* 2004). This event was also identified from Caribbean reefs (Blanchon and Shaw 1995) around 8 kyr with a magnitude of less than 10 m. MWP-1D began around 7 kyr BP and raised sea level to 2–3 m above present sea level and terminated at a Holocene highstand.

The sea level history for the west Pacific and the regional geologic setting of the study site are used to contextualize some scenarios that could explain the origin, timing, and mechanism of terrace formation in Pag-asa Reefs.

The Pag-asa terraces may have formed in several ways. One scenario is that the terraces were carved on old reef deposits through wave planation during episodes of relative stillstand through the overall sea level fall from the Marine Isotopic Stage (MIS) 5e highstand, between 130–119 kyr (Hearty *et al.* 2007), to MIS 2 or LGM. During the ensuing sea level rise from LGM to the present, these terraces were re-occupied by the sea during the ensuing rise of sea level due to deglaciation. This scenario requires minimal reef accretion post-LGM to preserve the wave-cut origin of the terraces. However, this scenario is unlikely as indicated by the luxuriant growth of corals in the region. Reef growth during the period between MIS 5e to MIS 2 (LGM) is likely intermittent owing to the overall trend of sea level fall punctuated by short-lived minor transgressions (MIS 5a and 5c) (Waelbroeck *et al.* 2002). During these episodes,

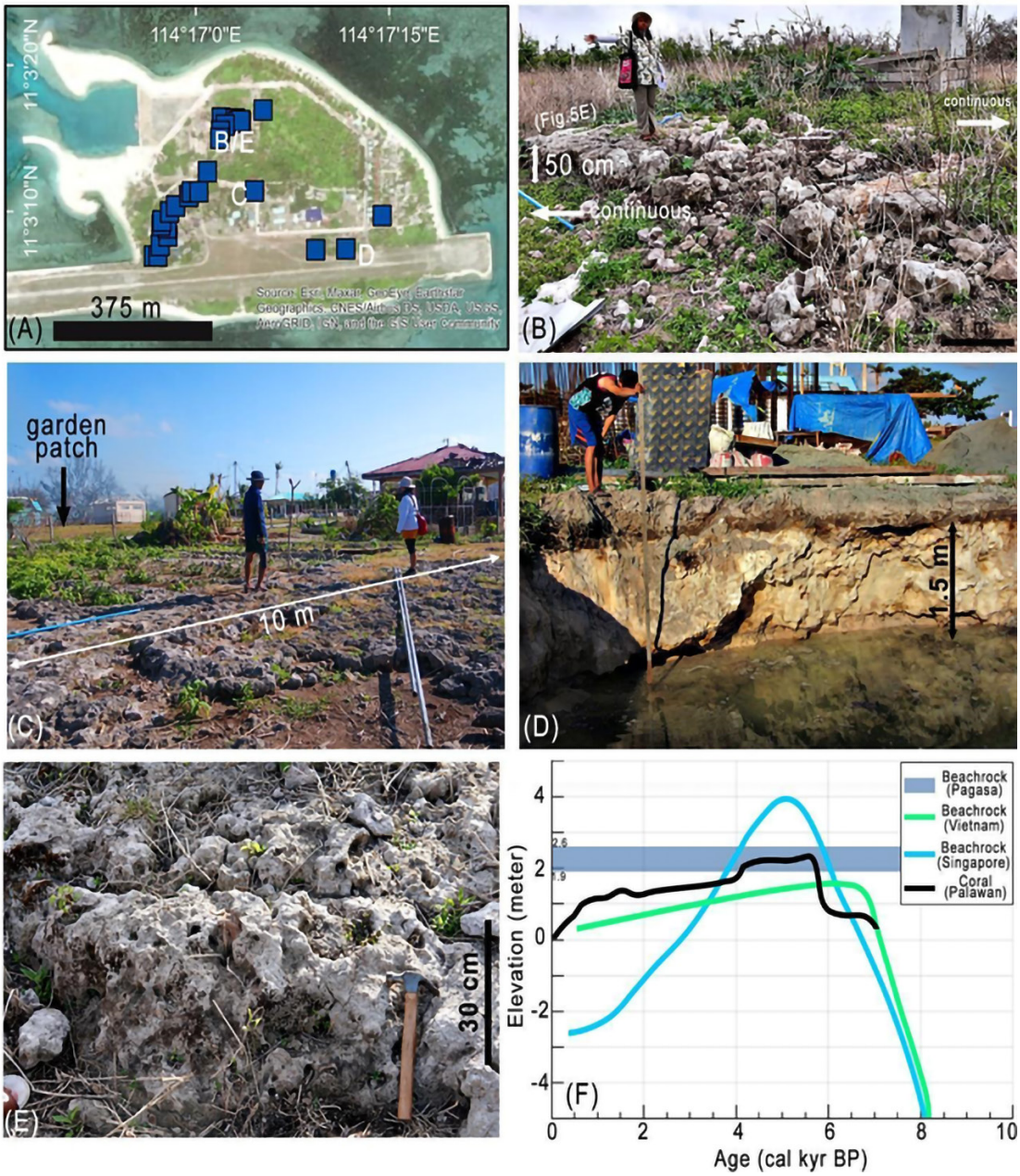

Figure 5. Beachrock exposures within Pag-asa Island. [A] Satellite image of Pag-asa Island with indicated sites of beach rock outcrops (blue square). [B–D] Sample beach rock outcrops within Pag-asa Island, whose locations are marked in [A]. [E] A closer picture of the beach rock outcrop in [B]. [F] Reconstructed paleo-sea level curves in Palawan (Maeda *et al.* 2009), Singapore (Chua *et al.* 2021), and Vietnam (Statteger *et al.* 2013) in the last 10,000 years. The legend indicates the proxy used by studies. The elevation range (with respect to msl) of the beach rock outcrops in Pag-asa Island is enclosed in the box.

reef formation was potentially minimal and negligible. When combined with wave planation during the ensuing sea level fall, they offer little to no surface that may serve as foundations for subsequent reef growth (Pastier *et al.* 2019).

The second scenario is that the Pag-asa terraces are coral reefs that formed and were submerged, and the deeper reefs, eventually drowned during the overall sea level rise after LGM (Figure 6). In this case, the terraces developed through keep-up or catch-up growth followed by progradation during stable sea level periods under an overall backstepping mechanism. Further, it is assumed that the post-LGM terraces grew on former reefs or wave-cut terraces that formed since or even prior to MIS 5e. Conceivably, the greater majority of the modern Pag-asa terraces are composed of post-LGM reefs with very little proportion of former reefs.

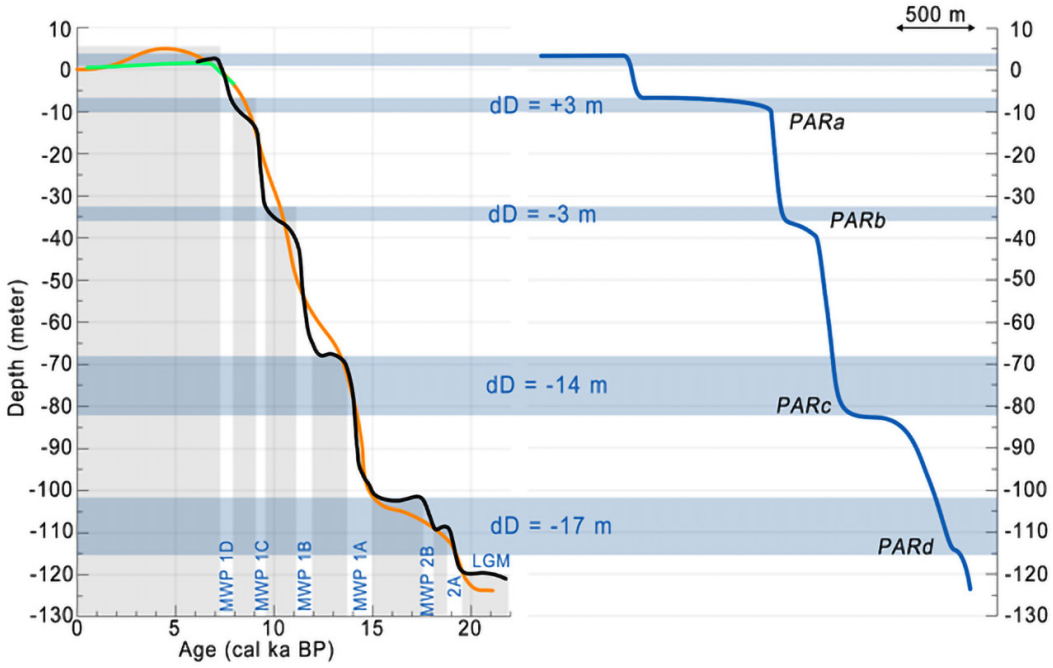

Figure 6. Morphological correlation between the existing post-LGM paleo-sea level curves (left panel) derived from North Yellow Sea (Liu *et al.* 2004, black line), Sunda Shelf (Hanebuth *et al.* 2009, orange line), and Vietnamese coast (Statteger *et al.* 2013, green line) and the Pag-asa reef terraces (right panel). The difference in depth (dD) of the Pag-asa terrace with its corresponding stillstand period was computed based on the North Yellow Sea curve, where (+) and (–) sign indicate shallower and deeper Pag-asa reef terraces respectively. The terraces are drawn based on their maximum widths and shallower depth limits.

The latter scenario is more reasonable because of the abundance of atolls in the area, which suggests luxuriant coral growth. Furthermore, the pattern of the Pag-asa terraces has a striking similarity with the sea level curve for the west Pacific (Liu *et al.* 2004) (Figure 6). In a scenario where MIS 5 or older reefs are preserved in the forereef slope of Pag-asa, several orders of terraces with varying widths and separations must be present, irrespective of depth. Thus, we interpret the Pag-asa terraces as having been formed during the post-LGM overall sea level rise.

The similarity of the morphology of the Pag-asa terraces to the sea level curve of Liu and co-authors (2004) provides a clue to the mechanism and timing of the formation of these terraces. The step-like morphology of the slopes of Pag-asa is likely due to the backstepping of reefs during rapid sea level rises and their eventual re-establishment in a more landward and higher position during an ensuing relative stillstand of sea level. Hence, terraces *PARa-d* are records of reef re-establishments during the stillstand periods following MWP-1C, MWP-1B, MWP-1A, and MWP-2B/2A, as identified by Liu and co-authors (2004). However, there is no clear morphological indicator of coral terraces that can be attributed to the LGM period. The height of the scarps separating the Pag-asa terraces approximates the magnitude of sea level rise estimated by Liu and co-authors (2004), which they attributed to MWP events. For example, from terrace *PARd* to *PARc,* the height of the scarp that is 33 m approximates a relative sea level rise of similar magnitude between the period of stillstands that formed the two terraces. Based on merged west Pacific paleo-sea level reconstructions, the relative sea level rise magnitude for MWP-1A is placed at ~ 22 m (Liu *et al.* 2004). The scarps separating *PARc* from *PARb* and *PARb* from *PARa* are 44 and 32 m, respectively. In relation, the magnitudes of relative sea level rise of MWP-1B and MWP-1C are 35 and 24 m, respectively (Liu *et al.* 2004). We attribute the increasing departure of the separation between the terraces and their corresponding magnitudes of sea level rise due to MWP to subsidence. The role of subsidence is explored in a later section.

The duration of the stillstand is a likely factor in the width or overall development of a terrace. Ideally, longer periods of stillstand would allow more extensive progradation of coral reefs, hence better-defined and wider terraces. The extant reef flat, terrace *PARa,* is the broadest of all the terraces whose maximum width is 1000 m. This is likely due to the overall length of time, of more than 7 kyr, during which sea level stood at or close to the present sea level. The relative stillstand following MWP-1B lasted for about 1.2 kyr; post MWP-1A for about 1.5 kyr, and post MWP-2B/2A for 4 kyr. For these stillstand periods,

the corresponding maximum widths of terraces *PARb-d* are 200, 230, and 40 m, respectively. A direct relationship between the width of the terrace and the duration of the stillstand can be established for the upper three terraces, but this fails for the deepest terrace, *PARd.* The poor development of the *PARd* reef can be due to the 2–4 ^{0}C cooler sea surface temperature during this period (Wei *et al.* 2007). Subsequently, the eustatic rise of sea level during MWP-1A further prevented reef vertical accretion by a catch-up, resulting in the demise of reefs that grew, albeit minimally, during the stillstand after the initial deglacial sea level rise (Montaggioni 2005). In Indo-Pacific sites with LGM records, the coral reefs only developed as thin veneers to a few meters thick [*e.g,* Mayotte (Dullo *et al.* 1998); Vanuatu (Cabioch *et al.* 2003)]. Presumably, these reef communities also drowned at the end of LGM (Montaggioni 2005). In Pag-asa, it is possible that there is also little to no reef accretion during LGM, hence the lack of a distinct morphological indicator.

The Role of Wave Exposure and Antecedent Topography

Although the morphology of the Pag-asa terraces is largely controlled by the eustatic sea level events, variation in terrace depth, width, extent, and slope is observed between the north- and south-facing forereef slopes of the atoll reefs. Based on the rose diagram of the monthly averaged wind speed over Pag-asa region (Figure 7), northeasterly winds in Pag-asa region comprise 51% of the recorded data, wherein 23% of which falls within the higher range of 8–11 ms^{-1}. Since the variation pattern is consistently dependent on the location of the terrace with respect to the whole atoll reef structure, it can be inferred that this is a function of wave exposure. In comparison, southwesterly winds comprise 38% of the recorded data, and only 2% of which falls within the 8–11 ms^{-1} range. The mean wind speed is 6.6 ms^{-1}, whereas the highest recorded monthly-averaged wind speed is almost 10 ms^{-1} oriented 20^0 NE. Occasional southeasterly winds also occur but at lower monthly-averaged wind speeds and only 9% of the record. This distribution is associated with monsoonal winds, indicating a stronger and more persistent Northeast Monsoon or *Amihan* and a relatively weaker and shorter duration Southwest Monsoon or *Habagat* activity. Typhoons that generally occur during *Habagat* can also impact the area. In air-sea interaction, the vector applied on the ocean surface by the wind is determined by the wind stress, responsible for the generation of surface waves (Smith *et al.* 1996) (Figure 7). Northeasterly wind stress makes up more than 50% of the record, 18% of which belongs to the higher wind stress range of 0.12–0.18 Nm^{-2}. Conversely, southwesterly wind stress is 39% of the record and only 3% falls within 0.12–0.18 Nm^{-2}. Higher wind stress values would result in greater wave height and more energetic waves.

The well-developed spur-and-groove features on the northern slopes of wPAR attest to the effect of strong and persistent swift NE winds on reef development. The NE winds also likely favored coral reef growth on the northern slopes of Pag-asa reefs, as indicated by its much broader terraces compared to those on the southern slopes. Even the extant reef flat is much broader on the northern side than on the southern side of Pag-asa Island. The pattern in Pag-asa reefs is consistent with what was observed by Hongo and Kayanne (2009) in the Ryukyu Islands, where exposure to high-energy waves promoted coral reef growth. However, in Hawaii, Grigg (1998) observed that only wave-sheltered sites had significant reef accretion, at 10–15 m thick, in contrast to wave-exposed stations with only a thin veneer of living corals.

The higher wave energy on the northern reefs is also expected to result in a deeper limit of wave scouring. This may explain the higher upper limit of the formation of terraces along the slopes on the south of the Pag-asa Reef. Chappell (1980) also reported that reefs in New Guinea exposed to energetic waves form at deeper sites than sheltered reefs. During the LGM, it is also likely that the NE winds were swifter because of the steeper temperature gradient between the equatorial region and higher latitude. In the west Pacific, stronger easterly winds during the peak of glaciation (Bush and Philander 1999) may have led to higher wave stress on corals, probably causing mortality due to breakage or abrasion. Hence, reef development may have been impeded on the windward side of Pag-asa, which could explain the discontinuous trace of terrace *PARd* towards the north.

Antecedent topography also played a role in the contrasting reef development between the north and south slopes of Pag-asa reefs. Overall, the south-facing slopes are steeper than the north-facing slopes at 58 and 29 °, respectively. A steeper slope would limit reef progradation and this is manifested by the much narrower terraces on the south-facing slopes. Multiple cycles of limited reef progradation and unrestricted vertical reef build-up on the south side of Pag-asa reefs resulted in the overall steeper slopes on the south.

Implication of Beach Rock Outcrops

The beach rocks found in the Pag-asa Island are always at or very close to land surface and are underlain by thick loose sands (Figure 5). This indicates that the beach sediments in Pag-asa lithified at supra-tidal settings to form beachrocks. Supratidal lithification can be caused by percolation and precipitation of seawater brought in during high-energy wave events. However, the elevation range of the exposed surfaces of the beach rocks, at 1.9–2.6 m

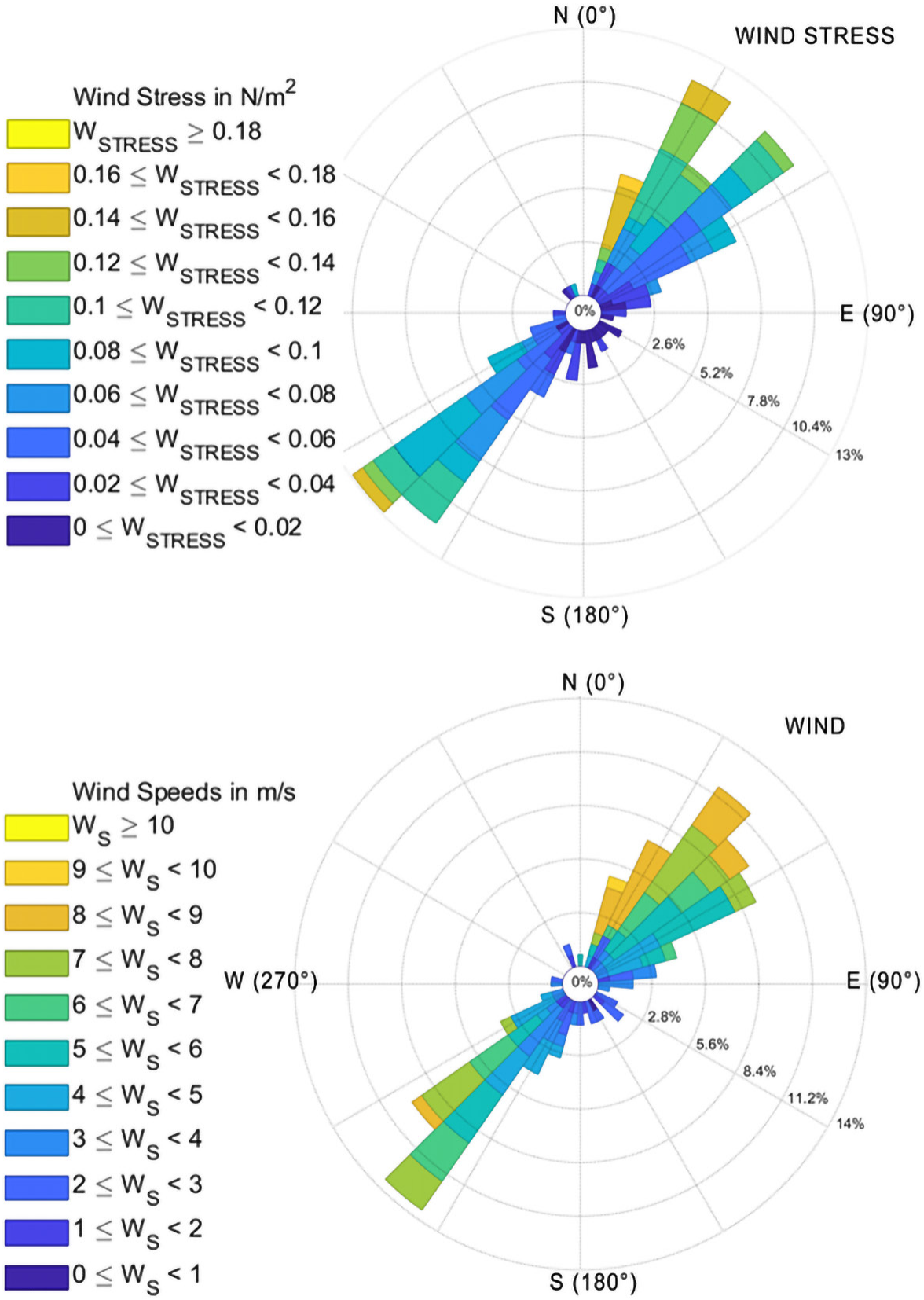

Figure 7. Wind rose diagrams showing monthly averaged wind stress (top) and wind speeds (bottom).

above msl, is generally higher than the elevations of extant storm berms which are about 1.5 m above msl along the southern shoreline and about 2.5 m above msl for beaches along the northern shoreline. Immediately landward of the extant storm berms, no lithification was observed.

The higher elevation of the beach rocks relative to the present storm berms around the island is consistent with a past sea level that is higher than the present. An MIS 5e origin for the beach rocks is unlikely because of the absence of any other indicators of emergent coral reefs and the loose nature of sand underneath them. A mid-Holocene highstand origin is more likely. The mid-Holocene highstand is extensively documented within the far-field Indo-Pacific region (Woodroffe and Horton 2005). In nearby Palawan Island, Maeda and co-authors (2009) – using a combination of marine notches, oyster shells attached to walls of caves, and corals with wave-cut tops that are exposed during low tide – reconstructed higher-than-present sea levels from about 7.5–1.5 kyr (Figure 5). They defined three highstands with the highest at 2.2–2.4 m above msl, which lasted from 5.5 to about 4.2 kyr.

Paleo-sea level reconstructions, specifically that of Maeda and co-authors (2009), suggest that the beach rocks should be at a higher elevation than their present elevation. The difference in elevation between the highest beach rocks and the present storm berms indicates a paleo-sea level that was only 0.6–1.1 m higher than the present. With the extant storm berms of Pag-asa Island having an average height of 1.75 m above msl and a paleo-sea level that was 2.2–2.4 m above the present msl, as suggested by Maeda and co-authors (2009), and supratidal lithification mechanism, beach rock formation would be at about 4.0–4.2 m above the present msl. The lower elevation of the beach rocks at Pag-asa Island can be due to a lower relative highstand in this part of WPS at the time of their formation; extensive erosion that may have ensued soon after the formation of the beach rocks; or due to subsidence that led to lower elevations. The first option is not supported by most of the reconstructed elevations of sea-level highstands. Along the coasts fringing the SCS, the Holocene highstand is placed at about 2 m (*e.g.* Palawan, Maeda *et al.* 2009; Vietnam, Statteger *et al.* 2013) to 4–5 m (Singapore, Chua *et al.* 2021) above the present msl. Second, erosion of the beach rock would require an even higher paleo-sea level and, thus, is not the likely cause. Erosion due to occasional strong typhoons is possible and erosion due to human activities, such as the use of beach rock material for the construction of the runway cannot be discounted. However, lowering of the elevation is counterintuitive to the desire to have high ground on a small, low-lying island. The possible role of subsidence is preferred and is explored in the next section.

Crustal Subsidence

The atolls in the WPS suggest long-term crustal subsidence in the region. Comparison of the terrace depth within Pag-asa with the west Pacific relative sea level curves (in Liu *et al.* 2004) shows that the Pag-asa terraces are consistently deeper, except for terrace *PARa,* which can be reasonably attributed to vertical accretion of coral reefs by keep-up, resulting to shallower reefs (Figure 6). There is also an increasing vertical separation with depth between the Pag-asa terrace depths and their corresponding stillstands. To estimate the magnitude of subsidence, we use the shallowest of the depth range of the southern terraces as well as the timing of the termination of the relative stillstand of sea level that corresponds to each terrace. The shallowest terrace depth best approximates the paleo-sea level at the time of their formation. Using this method, we compute a continuous crustal subsidence rate of 1.2 mm/yr from 15 to 12 kyr that declines to 0.3 mm/yr from 12 to 8 kyr, and possibly up to present times. On the other hand, the beach rock within the broad inner portion of Pag-asa Island which at present lies at a maximum elevation of 2.6 m above msl, could have been at 4.0–4.2 m above present msl during its formation. If the formation of the beach rocks is placed at the relative peak of the mid-Holocene highstand, between 5.5–4.2 kyr (Maeda *et al.* 2009), a subsidence rate of 0.3 mm/yr would have lowered the original elevation of these deposits by a minimum of 1.3 m yielding an elevation that should be at 2.9–2.7 m above present msl. Thus, the elevation of the beach rocks seems to support the idea of deceleration of subsidence towards the present.

Subsidence within the SCS region is well-established. At the northern thinned continental margin of SCS, in Qiongdongnan Basin, post-rift subsidence is observed to increase southward (Zhao *et al.* 2018). A rough calculation of their observed subsidence rate from 5.5 Ma to 0 provides a range of ~ 0.05–0.1 mm/yr. These rates are generally faster than the syn-rift subsidence rates. Possibly, subsidence within Pag-asa is also influenced by the varied crustal thickness of the thinned continental margin and post-rift crustal density changes. The mechanism for the apparently slowing subsidence rate is not certain. Perhaps, this indicates waning crustal subsidence due to a cooling crust.

Since subsidence is inferred based on morphological parameters, it is also possible that the deceleration of subsidence towards the present is an artifact of increased reef accretion around 12 kyr as promoted by warmer sea surface temperatures, increasing from 25–27 °C (Wei *et al.* 2007) congruous with the beginning of MWP-1B event. In this scenario, at least 8–11 m thick reef material within the Pag-asa terraces should have grown dramatically to keep up to a constant subsidence rate of 1.2 mm/yr. Based

on the modeled results in one of the atolls in the KIG, the subsiding Panganiban Reef (Meiji Atoll) has a 15-m thick reef accumulation within its atoll margins from 10.4 kyr to present, corresponding to the high-amplitude sea level rise during MIS 1 (Liu *et al.* 2022). Hence, a thick accumulation of Holocene reefs in Pag-asa is also possible.

Alternatively, in another scenario, the apparent slowing down of subsidence could be due to hydro-isostasy. Pag-asa, being in the far-field, could have undergone some uplift in the mid-Holocene due to reduced water load on the oceanic crust following ocean siphoning (Mitrovica and Milne 2002). The uplift could have offset the otherwise constant subsidence of the Pag-asa atolls.

Given all these considerations, we estimate that the long-term crustal subsidence in the region of Pag-asa reefs is between 1.2–0.3 mm/y. The atoll morphology of reef systems in the WPS indicates that subsidence is still taking place over the thinned continental crust 27–22 Ma post the last phase of opening of the SCS Basin (Sibuet *et al.* 2016). Variability of subsidence rates across the thinned continental crust offshore mainland Palawan can also be expected from likely variation in crustal thickness, similar to the case of the northwest part of the SCS (Zhao *et al.* 2018), and continuing influence of the transform shear zones cutting across it.

CONCLUSION

The morphology of the coral reef terraces on the forereef slopes of Pag-asa is an indicator of at least four episodes of sea level rise events post-LGM. Based on the extent of the coral reef terraces, it can be inferred that significant coral reef accretion started during the stillstand period following meltwater pulse-1A, for which the corresponding reef terrace now lies at a mesophotic depth of about 80 m. The extant reef flat possibly formed from about 9 kyr and kept pace by vertical accretion through the Holocene highstand periods. Beach rock exposures indicate the occurrence of a relative highstand that is greater than 2 m within the Pag-asa area during the mid-Holocene. High wave exposure is favorable to reef development as indicated by the more extensive coral reef terraces on the windward northern side of Pag-asa; however, we propose that high wave exposure combined with significantly cooler sea surface temperature hindered reef development and forced the pre-meltwater pulse 1A reefs to grow only at sheltered sites. Crustal subsidence of as much as 0.3–1.2 mm/yr is riding on the eustatic overall rise of sea level since the LGM. This has led to the development of the extant Pag-asa Atoll Reefs.

With sea level rise due to global warming and continuing subsidence, Pag-asa Island is threatened by coastal erosion, more frequent marine inundation, and groundwater salinization. These pose serious challenges to the Filipino community living on Pag-asa Island and other islands in the West Philippine Sea. Given that the reef provides not only sediment to nourish the beach but also as a wave breaker, the health of the reef should be safeguarded or better yet, improved. The existing groundwater resource can also be better protected through proper liquid waste handling and disposal. An expanded rainwater collection system should be put in place in each household and the design of building structures should adapt to the potential increase in frequency and height of marine inundation.

ACKNOWLEDGMENTS

This research was funded by the National Security Council through the i-RARE Project of Fernando P. Siringan, under the UPGRADE-CIA Program. The authors are also grateful to the two anonymous reviewers who gave detailed and constructive comments on the manuscript.

REFERENCES

ABBEY E, WEBSTER M, BEAMAN RJ. 2011. Geomorphology of submerged reefs on the shelf edge of the Great Barrier Reef: the influence of oscillating Pleistocene sea-levels. Marine Geology 288(1–4): 61–78.

BLANCHON P. 2011. Back-stepping. Encyclopedia of modern coral reefs. p. 77–84.

BLANCHON P, SHAW J. 1995. Reef drowning during the last deglaciation: evidence for catastrophic sea-level rise and ice-sheet collapse. Geology 23(1): 4–8.

BUSH AB, PHILANDER SGH. 1999. The climate of the Last Glacial Maximum: results from a coupled atmosphere-ocean general circulation model. Journal of Geophysical Research: Atmospheres 104(D20): 24509–24525.

CABIOCH G, MONTAGGIONI LF, FAURE G. 1995. Holocene initiation and development of New Caledonian fringing reefs, SW Pacific. Coral Reefs 14(3): 131–140.

CABIOCH G, DAVIES P, DONE T, GISCHLER E, MACINTYRE IG, WOOD R, WOODROFFE C. 2010. Encyclopedia of modern coral reefs: structure, form, and process. Springer Science & Business Media.

CAMOIN GF, WEBSTER JM. 2015. Coral reef response to Quaternary sea-level and environmental changes: State of the science. Sedimentology 62(2): 401–428.

CHAPPELL J. 1980. Coral morphology, diversity, and reef growth. Nature 286(5770): 249–252.

CHUA S, SWITZER AD, LI T, CHEN H, CHRISTIE M, SHAW TA, ... HORTON BP. 2021. A new Holocene sea-level record for Singapore. The Holocene 31(9): 1376–1390.

DE DECKKER P. 2016. The Indo-Pacific Warm Pool: critical to world oceanography and world climate. Geoscience Letters 3(1): 1–12.

DULLO WC, CAMOIN GF, BLOMEIER D, COLONNA M, EISENHAUER A, FAURE G, ... THOMASSIN BA. 1998. Morphology and sediments of the foreslopes of Mayotte, Comoro Islands: direct observations from a submersible. Spec Publs Int Ass Sediment 25: 219–236.

FAICHNEY ID, WEBSTER JM, CLAGUE DA, KELLEY C, APPELGATE B, MOORE JG. 2009. The morphology and distribution of submerged reefs in the Maui-Nui Complex, Hawaii: New insights into their evolution since the Early Pleistocene. Marine Geology 265(3–4): 130–145.

FAIRBANKS RG. 1990. The age and origin of the "Younger Dryas climate event" in Greenland ice cores. Paleoceanography 5(6): 937–948.

GRIGG RW. 1998. Holocene coral reef accretion in Hawaii: a function of wave exposure and sea level history. Coral Reefs 17(3): 263–272.

HEARTY PJ, HOLLIN JT, NEUMANN AC, O'LEARY MJ, MCCULLOCH M. 2007. Global sea-level fluctuations during the Last Interglaciation (MIS 5e). Quaternary Science Reviews 26(17–18): 2090–2112.

HONGO C, KAYANNE H. 2009. Holocene coral reef development under windward and leeward locations at Ishigaki Island, Ryukyu Islands, Japan. Sedimentary Geology 214(1–4): 62–73.

HORTON BP, KOPP RE, GARNER AJ, HAY CC, KHAN NS, ROY K, SHAW TA. 2018. Mapping sea-level change in time, space, and probability. Annual Review of Environment and Resources 43: 481–521.

LADD HS, INGERSON E, TOWNSEND RC, RUSSELL M, STEPHENSON HK. 1953. Drilling on Eniwetok atoll, Marshall islands. AAPG Bulletin 37(10): 2257–2280.

LIU J, WEBSTER JM, SALLES T, WANG S, MA Y, XU W, ... YAN W. 2022. The formation of atolls: new insights from numerical simulations. Journal of Geophysical Research: Earth Surface 127(8): e2022JF006812.

LIU JP, MILLIMAN JD, GAO S, CHENG P. 2004. Holocene development of the Yellow River's subaqueous delta, North Yellow Sea. Marine Geology 209(1–4): 45–67.

MAEDA Y, YOKOYAMA Y, SIRINGAN FP, QUINA G. 2009. Holocene relative sea-level fluctuations recorded in tidal notches along the Pacific coast of northern Luzon, Philippines. Journal of Geography 118(6): 1284–1291.

MITROVICA JX, MILNE GA. 2002. On the origin of late Holocene sea-level highstands within equatorial ocean basins. Quaternary Science Reviews 2120-22: 2179–2190.

MONTAGGIONI LF. 2005. History of Indo-Pacific coral reef systems since the last glaciation: development patterns and controlling factors. Earth-Science Reviews 71(1–2): 1–75.

NEUMANN AC, MACINTYRE I. 1985. Reef response to sea-level rise: keep-up, catch-up, or give-up. In: Proceedings of the fifth international coral reef congress Tahiti; 27 May–01 June 1985; volume 3: symposia and seminars (A). Antenne Museum-EPHE. p. 105–110.

ONG J, AGUDA N, JARAULA C, MATEO Z, PASCUA C, FORONDA J. 2000. Tidal effects on groundwater in a very small tropical island: a study on the groundwater resources of Pag-asa Island, Kalayaan Island Group.

PASTIER AM, HUSSON L, PEDOJA K, BÉZOS A, AUTHEMAYOU C, ARIAS-RUIZ C, CAHYARINI SY. 2019. Genesis and architecture of sequences of Quaternary coral reef terraces: insights from numerical models. Geochemistry, Geophysics, Geosystems 20(8): 4248–4272.

PEDOJA K, HUSSON L, BÉZOS A, PASTIER AM, IMRAN AM, ARIAS-RUIZ C, ... CHOBLET G. 2018. On the long-lasting sequences of coral reef terraces from SE Sulawesi (Indonesia): Distribution, formation, and global significance. Quaternary Science Reviews 188: 37–57.

PEREIRA D. 2022. Wind Rose. MATLAB Central File Exchange. Retrieved on 26 May 2022 from https://www.mathworks.com/matlabcentral/fileexchange/47248-wind-rose

QUIMPO TJR, CABAITAN PC, GO KTB, DUMALAGAN EE, VILLANOY CL, SIRINGAN FP. 2019. Similarity in benthic habitat and fish assemblages in the upper mesophotic and shallow water reefs in the West Philippine Sea. Journal of the Marine Biological Association of the United Kingdom 99(7): 1507–1517.

SCHLÜTER HU, HINZ K, BLOCK M. 1996. Tectono-stratigraphic terranes and detachment faulting of the South China Sea and Sulu Sea. Marine Geology 130(1–2): 39–78.

SHINN E. 1963. Spur and groove formation on the Florida reef tract. Journal of Sedimentary Research 33(2): 291–303.

SIBUET JC, YEH YC, LEE CS. 2016. Geodynamics of the south China sea. Tectonophysics 692: 98–119.

SMITH SD, FAIRALL CW, GEERNAERT GL, HASSE L. 1996. Air-sea fluxes: 25 years of progress. Boundary-layer Meteorology 78(3): 247–290.

STATTEGGER K, TJALLINGII R, SAITO Y, MICHELLI M, THANH NT, WETZEL A. 2013. Mid to late Holocene sea-level reconstruction of Southeast Vietnam using beachrock and beach-ridge deposits. Global and Planetary Change 110: 214–222.

WAELBROECK C, LABEYRIE L, MICHEL E, DUPLESSY JC, MCMANUS JF, LAMBECK K, ... LABRACHERIE M. 2002. Sea-level and deep water temperature changes derived from benthic foraminifera isotopic records. Quaternary Science Reviews 21(1–3): 295–305.

WEI G, DENG W, LIU Y, LI X. 2007. High-resolution sea surface temperature records derived from foraminiferal Mg/Ca ratios during the last 260 ka in the northern South China Sea. Palaeogeography, Palaeoclimatology, Palaeoecology 250(1–4): 126–138.

WOODROFFE SA, HORTON BP. 2005. Holocene sea-level changes in the Indo-Pacific. Journal of Asian Earth Sciences 25(1): 29–43.

ZHAO Z, SUN Z, SUN L, WANG Z, SUN Z. 2018. Cenozoic tectonic subsidence in the Qiongdongnan basin, northern South China Sea. Basin Research 30: 269–288.